Physicochem. Probl. Miner. Process., 59(1), 2023, 157409

http://www.journalssystem.com/ppmp

Physicochemical Problems of Mineral Processing

ISSN 1643-1049

New insights into pyrite-hydrogen peroxide interactions during froth flotation: experimental and DFT study

Qinbo Cao [1,2,3], Wenchao Yan [1], Shuming Wen [1,2], Dianwen Liu [1,3], Yanjun Li [1]

[1] Faculty of Land Resources Engineering, Kunming University of Science and Technology, Kunming 650093, Yunnan, China

[2] State Key Laboratory of Complex Nonferrous Metal Resources Clean Utilization， Kunming 650093, China

[3] Yunnan Key Laboratory of Green Separation and Enrichment of Strategic Mineral Resources, China

Corresponding authors: qinbocao@kust.edu.cn (Qinbo Cao), shmwen@126.com (Shuming Wen)

Abstract: Hydrogen peroxide (H_2O_2) is an efficient depressant for pyrite (FeS_2) flotation. However, the depressing mechanism of H_2O_2 is not fully understood. In this paper, the depressing capacity of H_2O_2 for pyrite was examined by flotation tests. Results revealed that pyrite flotation could be inhibited by H_2O_2 at pH 6.4. The pyrite powder in H_2O_2 solution enhanced the release of O_2 from H_2O_2. However, the O_2 concentration in the solution was less than that of H_2O_2; thus, H_2O_2 is the major oxidant in the solution. Moreover, density functional theory calculations were performed to study the interactions between H_2O_2 and hydrated pyrite (100) surface. The H_2O_2 molecule tended to react with the pyrite surface to generate one S=O bond and an H_2O molecule. The possible binding models of O_2 molecules on the pyrite (100) surface were also studied for comparison. The O_2 dissociation on the pyrite surface was more favorable than the adsorption of O_2 as a whole. In addition, the orbital interaction in the S=O bond raised from the reaction of H_2O_2/O_2 with the pyrite surface was also investigated by the density states analysis. These results provide some insights into the oxidizing effect of H_2O_2 in pyrite flotation.

Keywords: hydrogen peroxide, oxidization, pyrite flotation, adsorption models, DFT

1. Introduction

Pyrite (FeS_2) is a prevalent sulfide commonly coexisting with other sulfides in a multiple sulfides deposit (Gisbert et al., 2022; Han et al., 2022). Pyrite in a concentrate of other sulfides increases the ferry and sulfur grades of the concentrate. Consequently, such concentrate fails to reach the smelting requirements. Thus, pyrite is treated as a gangue mineral (Muravyov, 2019) and separated from other sulfides, such as chalcopyrite or galena (Lü et al., 2018).

Pyrite has a good natural floatability (Derycke et al., 2013); thus, depressants must be used to prevent pyrite flotation. Lime (CaO) is widely used to depress pyrite in the industry (Mu et al., 2016), owing to its low price and wide resources. However, when the pyrite content in an ore is extremely high, lime cannot inhibit pyrite flotation efficiently, because of the lower solubility of lime. In this regard, a large number of organic and inorganic depressants have been developed to separate pyrite from other sulfides (Bai et al., 2021; Khoso et al., 2019b). Some high-molecular-weight polymers could be used as inhibitors for pyrite flotation, such as galactomannan (Jin et al., 2021), tricarboxystarch (Khoso et al., 2021), and sodium humate (Bai et al., 2022). In addition, several low-molecular-weight organics, such as citric acid, are also efficient pyrite flotation inhibitors (Liu et al., 2021). For a run-of-mine ore, organic depressants always show a poor selectivity for pyrite, as the slime in the ore may also adsorb organic reagents resulting in a high dosage of reagents. Thus, more efficient reagents are still needed to inhibit pyrite flotation.

Inorganic oxidants can be employed as pyrite flotation inhibitors, as pyrite is more sensitive to oxidants compared with other sulfides (Hong et al., 2017; Mu et al., 2016; Zhang et al., 2023). H_2O_2 is an efficient oxidant for pyrite (Liu et al., 2022). The application of this oxidant is attracting considerable attention (Chen et al., 2022; Suyantara et al., 2018), owing to its minimal impact on the environment and

DOI: 10.37190/ppmp/157409

low price. H_2O_2 could oxidize pyrite in the wide pH of 5–11 (Forson et al., 2021; Khoso et al., 2019a). This oxidant could also be used in the special flotation of pyrite using seawater (Yang et al., 2022). H_2O_2 is also generated on the pyrite surface during the wet grinding of pyrite (Javadi Nooshabadi et al., 2013). In these works, the final oxidation products, including FeO, FeOOH, $FeSO_4$, S_0, S^{2-}, and S_n^{2-}, have been well established by experimental methods. However, the interaction model of the H_2O_2 molecule on the pyrite surface is not fully understood. Moreover, H_2O_2 is not extremely stable in water and may dissociate into O_2 and H_2O. Since O_2 is also an oxidant for pyrite, it is still uncertain whether H_2O_2 or O_2 is the major oxidant in the H_2O_2–pyrite system.

On the other hand, because it is challenging for experimental approaches to reveal the binding features of oxidants on pyrite surface at the atomic level, researchers have used the Density functional theory (DFT) calculations to investigate the flotation mechanism of pyrite. The electronic structure and optical properties of pyrite can be probed by DFT calculations (Li et al., 2018). In addition, Jianhua Chen et al. used DFT calculation to study the adsorption features of collectors and the oxygen molecule on clean pyrite surfaces (Chen et al., 2013; Huang et al., 2017). The effect of impurities on the electronic and structural details of pyrite could be revealed by DFT calculations (Chen et al., 2014a; Li et al., 2011). These works were carried out on clean pyrite surfaces without H_2O molecules. While, the impact of H_2O on the adsorption behavior of reagents on mineral surfaces is receiving increasing attention since the flotation processes are carried out in water (Chen et al., 2014b; Foucaud et al., 2019). It was found that the H_2O and O_2 molecules in the pulp may react with the pyrite and galena surfaces to generate •OH radical and H_2O_2 (Javadi Nooshabadi and Rao, 2016). This finding has been verified by DFT results (Chen et al., 2017). These findings indicate that H_2O on the pyrite surface plays an important role in the oxidation process of pyrite. Furthermore, the H_2O molecule interacts with the Fe atom on the pyrite surface, which may influence the interaction between an oxidant and the pyrite surface (Javadi Nooshabadi et al., 2013). Whereas, few researchers have addressed the interaction between H_2O_2 on a pyrite surface with H_2O molecules, and thus the binding features of H_2O_2 on the hydrated pyrite surface are not fully understood.

This paper aimed to extend knowledge about the reaction of H_2O_2 with the pyrite surface. First, the depressing capacity of H_2O_2 for pyrite was examined by flotation tests. Dissolved oxygen (DO) concentration in the H_2O_2–pyrite system was also measured to determine the major oxidant in the system. Furthermore, the binding features of H_2O_2 and O_2 on the hydrated pyrite (100) surface were also studied by density functional theory (DFT) calculations.

2. Materials and methods

2.1. Minerals and reagents

Pure pyrite pebbles were hand-picked from a pyrite deposit in Yunnan Province, China. The X-ray diffraction (XRD) pattern of the pyrite sample is plotted in Fig. 1, where only pyrite was found in this sample. XRF results are also used to conform the purity of the sample (Table 1). The XRD results suggested that the pyrite crystal is cubic, and belongs to the Pa-3 space group. Analytical-grade H_2O_2 solution (30%) and sodium ethyl xanthate (SEX) were purchased from Sinopharm Chemical Reagent Co., Ltd. Terpenic oil was obtained from Henan Alfa Chemical Co., Ltd. and used as a frother in the flotation tests.

2.2. Flotation tests

Pyrite (-74+38 μm, 2g) was used for each flotation test. Flotation experiments were performed by an XFGC II flotation machine equipped with a 40 mL flotation cell (Jilin Province Ore Exploration Machinery Factory, China). The pyrite was treated with an H_2O_2 solution for a desirable time before the flotation test, after which the sample was transferred into the flotation cell (5% of solid concentration). The pH of the suspension was 6.4, which was adjusted by dilute NaOH and HCl solutions (1×10^{-4} mol/dm^3). Furthermore, SEX and frother (50 mg/dm^3) were added to the flotation cell. The conditioning times for SEX and frother were 2 and 1 min, respectively. The stirring speed of the flotation machine was set as 1800 r/min and the air flowrate was 1.16 dm^3/min. The flotation time was controlled as 2 min. Foam and underflow products were collected, dried and weighed to calculate the recovery. The flotation tests were performed at 23℃. Each flotation test was repeated three times.

Table 1. XRF results of pyrite sample used in this work

Element	Fe	S	Al	Ca	Si	Zn
wt.%	43.98	47.79	0.07	0.71	0.67	0.05

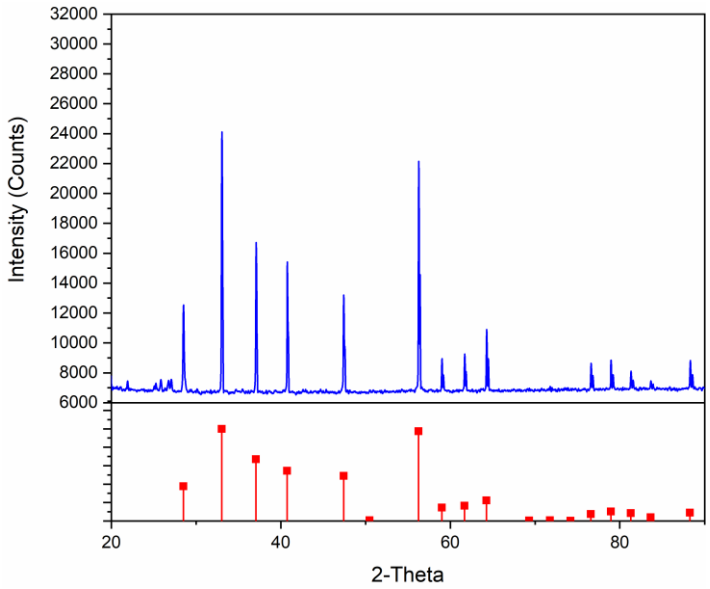

Fig. 1. XRD pattern of (a) pyrite sample and (b) standard XRD PDF card (#65-3321) of pyrite

2.3. DO concentration determination

A HACH (HP30D, US) instrument was employed to determine the DO concentrations of the H_2O_2 solution with pyrite powder. The electrode was washed with abundant deionized (DI) water before the test. Then, 2 g pyrite powder (−74+38 μm) was added to 40 mL of DI water, where the electrode of the instrument was placed. A desired amount of H_2O_2 was further placed into the pyrite suspension, and the DO of the pyrite solution was detected by the instrument in real time.

2.4. DFT calculations

DFT calculations were carried out with the Cambridge Sequential Total Energy Package (CASTEP) (Segall et al., 2002). The exchange and correlation potentials were treated by generalized gradient approximation (GGA) with the Perdew–Burke–Ernzerhof functional scheme (Perdew et al., 1996; Perdew and Zunger, 1981). The valence electronic configurations for the elements during the calculations are Fe $3d^6 4s^2$, S $3s^2 3p^4$, H $1s^1$, and O $2s^2 2p^4$. The electron-ion interactions were considered by the ultrasoft pseudo-potential (Francis and Payne, 1990). The kinetic energy cutoff in the DFT calculations was 580 eV. According to our convergence test results of pyrite surface, a cutoff energy of 380 eV is sufficient for the calculation. However, the cutoff energy is 570 eV under the fine-quality setting for the system, thus a cutoff energy of 580 eV was chosen in this work. Besides, Hubbard correction was not used in this work, and should be considered in further study. Brillouin zone integrations were performed with a 3×3×1 k-point mesh and spin-polarization was also applied during the calculations. The convergence criteria for the geometry optimization were: a maximum displacement of 0.001 Å, a maximum force of 0.03 eV/Å, a maximum energy change of 1×10^{-5} eV/atom and maximum stress of 0.05 GPa. In addition, the self-consistent field convergence tolerance was set to 1×10^{-6} eV/atom. These parameters were sufficient to achieve a numerical convergence as tested through the energy calculation of the slab model.

A (2×2) pyrite (100) surface model was cleaved from the bulk pyrite model for further study as this surface is the most stable surface (Chen et al., 2014b). The surface slab model contained nine atomic layers and a 15 Å vacuum layer. The atoms in the last layer were fixed in their bulk positions and the rest of the atoms were allowed to relax during the geometry optimization. The adsorption energy (ΔE_{ads})

of an adsorbate on the pyrite (100) surface was calculated as follows:
$\Delta E_{ad}=(E_{slab+Nadsorbate}-E_{slab}-nE_{adsorbate})/n$,
where E_{slab} and $E_{adsorbate}$ are the total energies of the pyrite (100) model and the adsorbate (H_2O, H_2O_2 or O_2) before the interaction, respectively; $E_{slab+Nadsorbate}$ refers to the energy of the surface model with adsorbates; and n is the number of adsorbate on the surface.

3. Results and discussion

3.1. Depressing behavior of H_2O_2 for pyrite flotation

Flotation tests were performed to re-examine the depressing behavior of H_2O_2 for pyrite flotation, and the results are reported in Fig. 2. The recovery of natural pyrite reached 71.4% without the collector, suggesting that natural pyrite has good floatability. Furthermore, the addition of SEX improved pyrite recovery. Pyrite recovery increased to 90.3% with 2×10^{-4} mol/dm^3 SEX. However, pyrite recovery was only raised by 3.2%, as the SEX concentration was increased from 2×10^{-4} mol/dm^3 to 4×10^{-4} mol/dm^3. Thus, 2×10^{-4} mol/dm^3 SEX is high enough for pyrite flotation. When the pyrite sample was oxidized by 2×10^{-3} mol/dm^3 H_2O_2 for 2 min, the recovery was reduced by 21%–30% for each examined SEX concentration. Such results indicate that oxidization with 2×10^{-3} mol/dm^3 of H_2O_2 can inhibit pyrite flotation to a certain degree.

The effect of H_2O_2 concentration on pyrite was further evaluated by flotation tests with a SEX concentration of 2×10^{-4} mol/dm^3 to probe the depressing capacity of H_2O_2. When the pyrite was oxidized by H_2O_2 for 2 min, the recovery sharply decreased with the increase in H_2O_2 concentration (Fig. 3A). As a result, pyrite recovery was lowered to 41.5% by 3×10^{-3} mol/dm^3 H_2O_2. However, the further increase in H_2O_2 concentration did not cause a reduction in pyrite recovery. Moreover, oxidation time may also influence the depressing capacity of H_2O_2. The pyrite recovery was reduced obviously from 85.2% to 31.1% by 3×10^{-3} mol/dm^3 H_2O_2 in the oxidization time of 0–3 min. Pyrite recovery reached a stable value (nearly 30%, Fig. 3B) at an oxidation time above 3 min. The results indicate the pyrite flotation could be inhibited by 3 min of H_2O_2 oxidization (3×10^{-3} mol/dm^3).

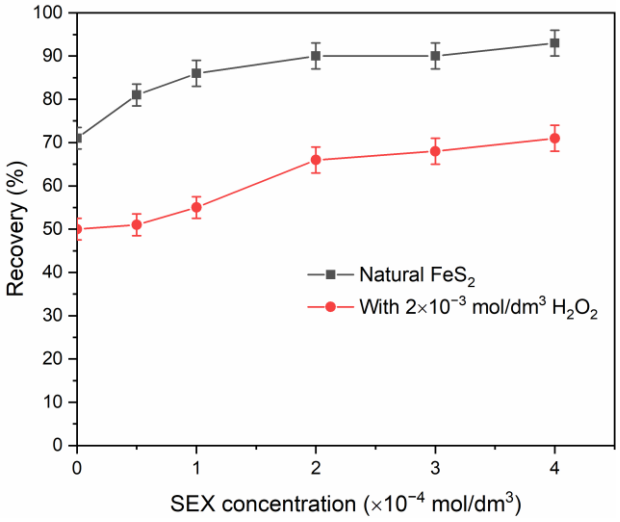

Fig. 2. Flotation recoveries of natural and oxidized pyrite by 2×10^{-3} mol/dm^3 H_2O_2 (2 min of oxidization) depending on the SEX concentration

Khoso et al. reported that the pyrite recovery was 20% when pyrite was oxidized by 3×10^{-3} mol/dm^3 of H_2O_2 for 3 min (Khoso et al., 2019a). Our result at the same oxidization parameters was 10% higher than the report of Khoso et al. Their flotation tests were carried out under pH 9. Differently, the pH of the H_2O_2 solution was not regulated and was 6.4 in the present work. The difference in pH conditions accounts for the discrepancy in pyrite recoveries in these works. Philip Forson et al. found that H_2O_2 could not completely depressed the pyrite flotation using potassium amyl xanthate or sodium diisobutyl dithiophosphateat as a collector pH 6.4 (Forson et al., 2021). Our study showed that H_2O_2 could prevent the H_2O_2 flotation at such pH. Such difference may be due to the different collectors used

in these works.

On the other hand, Miller et al. observed that iron oxide/hydroxide islands coated the pyrite surface when pyrite was oxidized by H_2O_2 (Jin et al., 2015). These species generate a hydrophilic surface, which deteriorates pyrite flotation.

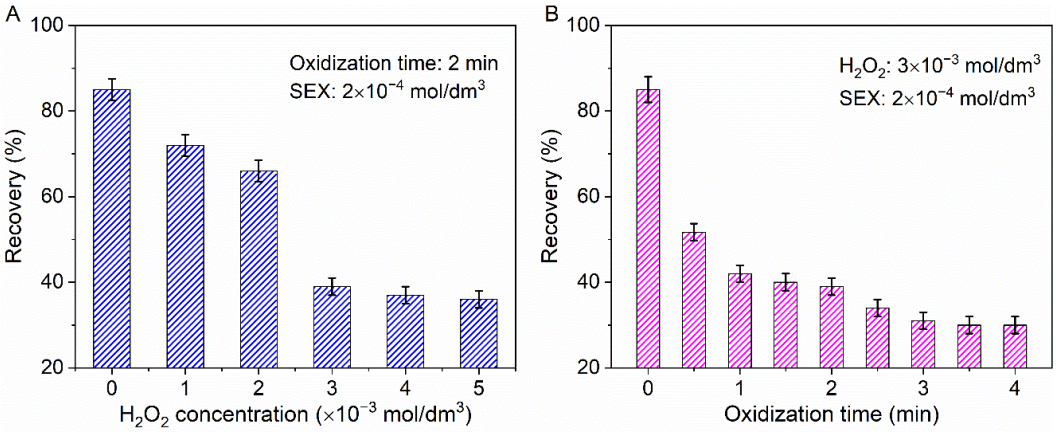

Fig. 3 Flotation recoveries of oxidized pyrite as a function of H_2O_2 concentration (A) and oxidization time (B)

3.2. DO concentrations in pyrite slurry

H_2O_2 is unstable in the solution and may dissociate into H_2O and O_2. To examine the stability of H_2O_2 in the pyrite slurry, the DO levels of pyrite-H_2O_2 suspension at various conditioning times were measured in this part.

As for 3×10^{-3} mol/dm^3 H_2O_2 solution without pyrite, the DO concentration gradually increased from 8.21 mg/dm^3 to 22.00 mg/dm^3 in 9 min (Fig. 4). It should be mentioned that 22.00 mg/dm^3 is the upper limit of the instrument. A similar trend of DO concentrations was observed for 4×10^{-3} mol/dm^3 H_2O_2 solution. The DO concentration in 4×10^{-3} mol/dm^3 H_2O_2 solution at each measurement time was close to that in the 3×10^{-3} mol/dm^3 H_2O_2 solution. By contrast, when pyrite was added to the 3×10^{-3} or 4×10^{-3} mol/dm^3 H_2O_2 solution, the DO concentration reached 20.00 mg/dm^3 in a much shorter time (3−5 min), compared with that without pyrite. Such results indicate that pyrite in H_2O_2 solution stimulates the dissociation of H_2O_2 into O_2 (Reaction 1).

$$2H_2O_2 \rightarrow 2H_2O+O_2 \quad (1)$$

On the other hand, the DO concentration in the 3×10^{-3} mol/dm^3 of H_2O_2 solution with pyrite was 18.48 mg/dm^3 (5.44×10^{-4} mol/dm^3) after 3 min of conditioning. Such DO concentration was much lower than the initial H_2O_2 concentration (3×10^{-3} mol/dm^3). Although DO is also an effective oxidant for pyrite, considering the relatively lower concentration of DO, H_2O_2 is expected to be the major oxidant in the pyrite−H_2O_2 suspension.

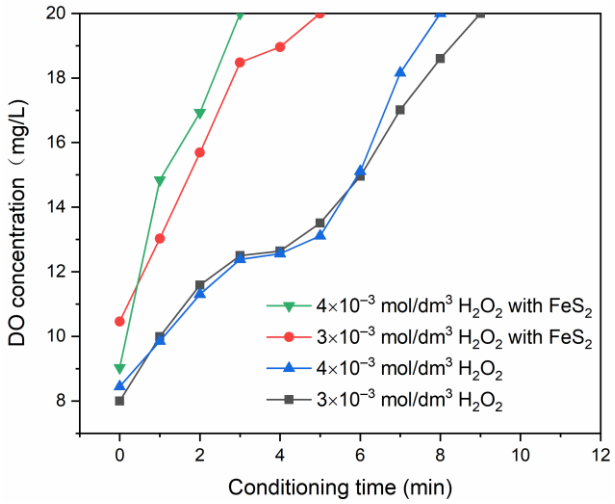

Fig. 4. DO concentrations of H_2O_2 solutions with and without pyrite as a function of conditioning time

3.3. DFT calculation study

The above flotation results and previous works demonstrated that H_2O_2 could be used as a pyrite depressant (Khoso et al., 2019a). The possible adsorption models of H_2O_2 on the pyrite (100) surface were investigated in this part, to further understand the interaction between H_2O_2 and the pyrite surface. The interaction models of the O_2 molecule were also probed, as O_2 is also an important oxidant in the H_2O_2 solution.

The H_2O_2 structure was optimized with the CASTEP code (Fig. 5). As for the optimized H_2O_2 structure, the bond angle of O–O–H was 98.5° and the bond length of O–O was 1.48 Å. The geometrical parameters of H_2O_2 agree well with the previous results (Tarchouna et al., 2006).

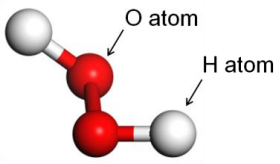

Fig. 5. Optimized structure of the H_2O_2 molecule

The H_2O-covered pyrite (100) model was used to study the interaction between H_2O_2/O_2 and the pyrite surface (Fig. 6). Five H_2O molecules were initially placed on the top sites of Fe and S atoms on the pyrite surface. While these H_2O molecules were located stably on the Fe sites on the surface after the geometry optimization. The ΔE_{ad} of H_2O molecules was -0.60 eV, which is in line with a previous report (Chen et al., 2014b). This result infers that the adsorption of H_2O molecules on the pyrite surface is energetically favorable. On the other hand, previous work also reported that the H_2O molecule bonds to Fe atoms rather than S atoms on the pyrite surface (Chen et al., 2014b). Therefore, our H_2O-covered model is reasonable to present the hydration state on the pyrite surface. Such treatment has been used to study the hydration state of rutile surface (Perron et al., 2007). In addition, interacting atoms on the pyrite (100) surface were numbered for the convenience of reporting the adsorption structures, as shown in Fig. 7.

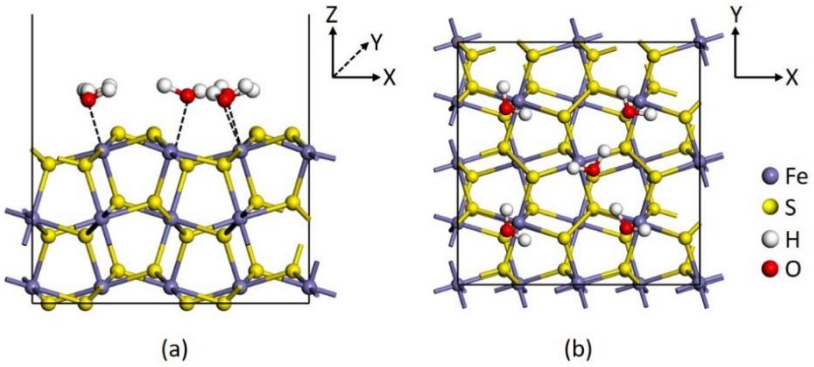

Fig. 6. Side (a) and top (b) views of the H_2O-covered pyrite (100) surface model used in this work. Only the top layer of pyrite and H_2O molecules are shown in the figure of the top view

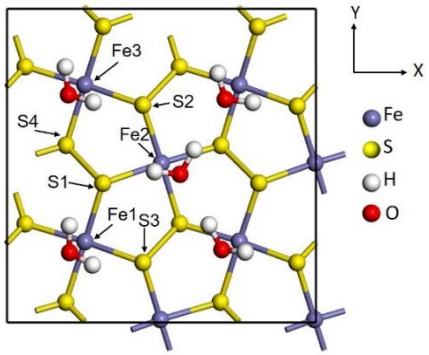

Fig. 7. Interactional atoms on the hydrated pyrite (100) surface

3.3.1. Geometrical features of H_2O_2 on the hydrated pyrite surface

An H_2O_2 molecule was placed at various sites on the hydrated pyrite surface to search the possible binding models. The orientation of H_2O_2 at each site (vertical or parallel orientation) was also considered during the calculations.

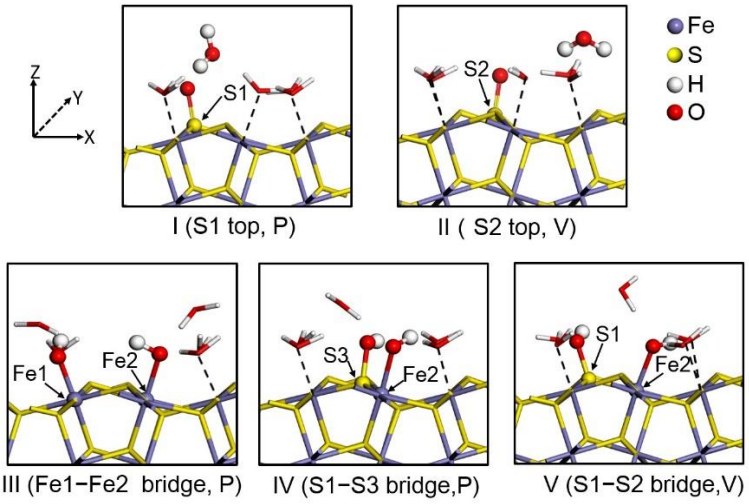

Fig. 8. Side views of the binding structures (I–V) of H_2O_2 at various sites of the hydrated Fe_2S surface (P and V mean parallel and vertical orientations, respectively). Atoms from H_2O_2 and interactional atoms are shown in a ball style, and other atoms are shown in a stick style to better view the structure

Five adsorption structures were generated on the hydrated pyrite surface (i.e., structures I–V in Fig. 8). The ΔE_{ad} results and surface products for each structure are summarized in Table 1. For structure I, the H_2O_2 molecule was initially placed on the top site of the S1 atom with parallel orientation. This H_2O_2 molecule dissociated into an O atom and an H_2O molecule through geometry optimization. Moreover, the O atom from H_2O_2 interacted with the S1 atom, forming an S1=O species. Similarly, when the H_2O_2 molecule was placed on the top site of S2, S2=O and one H_2O molecule were formed on the hydrated pyrite surface (structure II). This binding model was not found on the clean pyrite surface without H_2O molecules in a previous work (Zhang et al., 2018). The H_2O molecules on the pyrite seemed to affect the interaction behavior between H_2O_2 and the pyrite surface. Thus, the role of surface H_2O molecules needs to be considered in the DFT calculations.

H_2O_2 dissociation generated two OH groups when the H_2O_2 molecule was located at the bridge site of Fe1 and Fe2 at the initial stage (paralleling to the surface). These OH groups displaced two H_2O molecules binding to Fe1 and Fe2 atoms, which generated Fe1–OH and Fe2–OH bonds, respectively. As a result, the displaced H_2O molecules migrated away from the pyrite surface. Similar interaction models were observed when the H_2O_2 molecule was located at the bridge site of S1–S3 or S1–Fe2, where the OH groups were produced from the H_2O_2 molecule and bonded to Fe or S atoms on the pyrite surface.

Table 1. ΔE_{ad} and surface products of H_2O_2 at various sites on the hydrated pyrite surface

Structure	Site	H_2O_2 orientation	ΔE_{ad} (eV)	Surface products
I	S1 top	Parallel	−3.50	S1=O, H_2O
I	S2 top	Vertical	−3.42	S2=O, H_2O
III	Fe1 and Fe2 bridge	Parallel	−3.18	Fe1–OH, Fe2–OH
IV	S1 and S3 bridge	Parallel	−2.68	S3–OH, Fe2–OH
V	S1 and Fe2 bridge	Vertical	−2.55	S1–OH, Fe2–OH

Moreover, the ΔE_{ad} values of structures I and II are lower than those of the other structures (Table 1). The results suggest that structures I and II were more stable. The oxidization of the S atom occurred in structures I and II. Differently, Fe–OH species was generated in the other structures. Such results implied that the oxidization of S atoms on the pyrite surface occurred prior to that of Fe atoms.

3.3.2. Geometry features of O_2 on the hydrated pyrite surface

Above DO tests revealed that pyrite in the slurry enhanced the relation of O_2 from H_2O_2. The binding features of the O_2 molecule on the hydrated pyrite surface were also investigated for compaction, because pyrite can be oxidized by O_2 in the slurry.

Five adsorption structures were found on the hydrated pyrite (100) surface (i.e., structures VI–X, Fig. 9). In structure VI, two S=O bonds were generated at the bridge site of S1 and S2 (Table 2), where the O_2 molecule was placed at this site parallel to the surface in the initial structure. The ΔE_{ad} of this structure was the lowest among structures VI–X, suggesting that this adsorption model was the most stable for the adsorption of O_2 on the hydrated pyrite surface. A similar adsorption model was found on a clean pyrite surface (Rozgonyi and Stirling, 2015). The O_2 molecule could adsorb at the bridge site of Fe1–S2 or S2–S4, where the O_2 molecule was dissociated into two O atoms. As a result, S–O or Fe–O bonds were generated at these bridge sites. Nonetheless, the O_2 molecule could be linked to the S1 atom without dissociation, as shown in structures IX and X. However, the ΔE_{ad} values of structures IX and X were higher than that of structure VI, which indicates that the O_2 molecule has a high tendency to dissociate into two O atoms on the hydrated pyrite surface.

In addition, the ΔE_{ad} of structure VI was lower than that of structure I (the most stable structure of H_2O_2 on the pyrite surface), which suggests that the oxidizing capacity of O_2 and the pyrite surface was stronger. Moreover, H_2O_2 is expected to be the dominant oxidant in the H_2O_2–pyrite system, owing to the lesser amount of O_2 compared with H_2O_2.

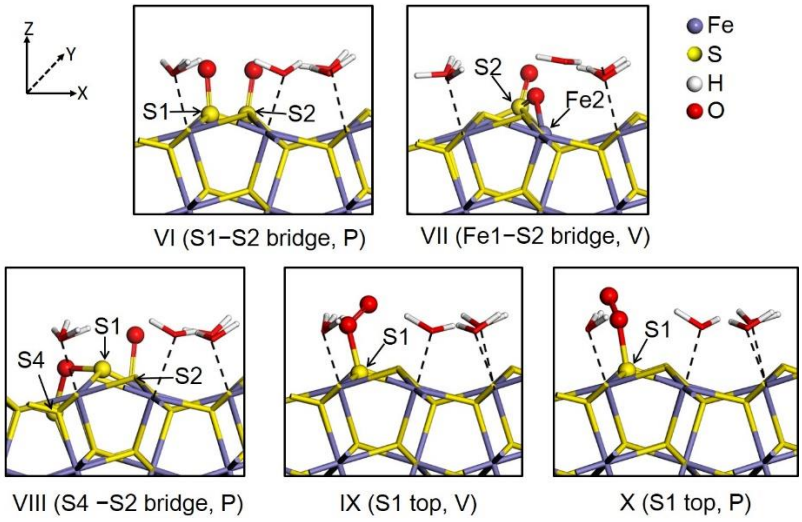

Fig. 9. Side views of the binding structures (VI–X) of O_2 at the hydrated Fe_2S surface (P and V mean parallel and vertical orientations, respectively). Atoms from O_2 and interactional atoms are shownan a ball style, and other atoms are shown in a stick style to better view the structure

Table 2. ΔE_{ad} and surface products of O_2 at various sites of H_2O-covered pyrite surface

Structure	Site	O_2 orientation	ΔE_{ad} (eV)	Surface products
VI	S1 and S2 bridge	Parallel	−5.11	S1=O, S2=O
VII	Fe2 and S2 bridge	Vertical	−3.30	S2=O, S2–O–Fe2
VIII	S4 and S2 bridge	Parallel	−3.11	S2=O, S1–O–S4
IX	S1 top	Vertical	−2.28	S1–O–O
X	S1 top	Parallel	−1.70	S1–O–O

3.3.3. Partial density of states (PDOS) analysis

The geometry-optimization results showed that the interaction between H_2O_2 or O_2 molecule and the hydrated pyrite surface generated new S–O/S=O bonds. Here, the chemical natures of S−O/S=O bonds were further studied by PDOS analysis, since such analysis could reveal the hybridization of atomic

orbitals in a chemical bond. Only the results for structures I and VI were reported, as these structures were the most stable for H_2O_2 and O_2 adsorption.

As for structure I, an S1=O bond was formed on the surface caused by the reaction of H_2O_2 with the hydrated pyrite surface. The valence band of the O in the H_2O_2 molecule and S1 atoms from −10 eV to −5 eV consisted of O 2p and S 3p orbitals before the interaction (Fig. 10). The reaction of the O atom with the S1 atom altered the orbital states of these atoms. As a result, the O 2p and S 3p orbitals were well overlapped in the energy level from −10 eV to −5 eV. Moreover, the O 2s state matched the S 3s states at −12.1, −14.3, −20.9, and −21.8 eV. Such results suggest that a hybridization occurred among O 2p, S 3p, O 2s, and S 3s orbitals.

In the case of structure VI, two S=O bonds (S1=O and S2=O) were generated on the pyrite surface because of the dissociation of the O_2 molecule. The PDOS results of these bonds were similar; thus, the results of S1–O were reported in this part (Fig. 11). The O 2p states of the interactional O atom in the free O_2 molecule were located at 0, −6.8, and −7.6 eV, whereas the O 2s states were found in the deeper

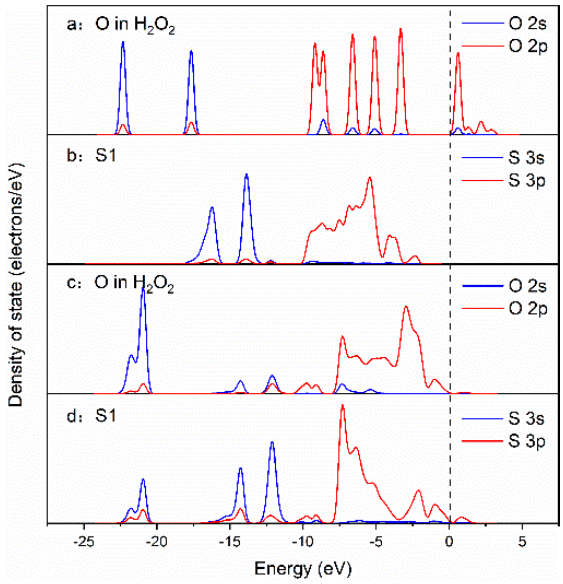

Fig. 10. PDOS of S1 atom on the pyrite surface and O atom in H_2O_2 in structure I before (a, b) and after (c, d) the interaction

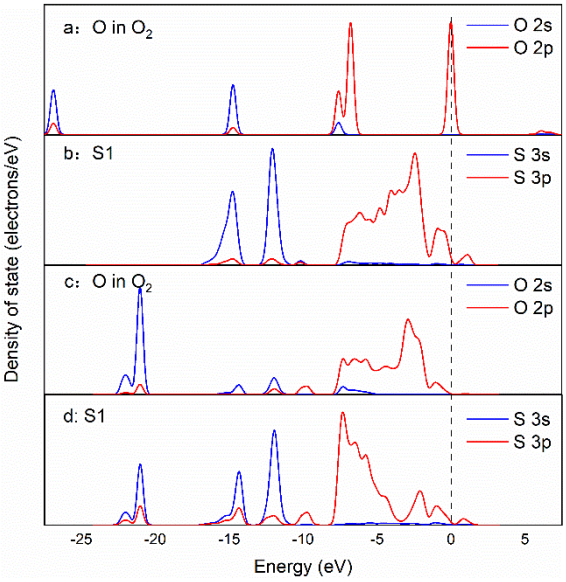

Fig. 11. PDOS of S1 atom on the pyrite surface and O atom in H_2O_2 in structure VI before (a, b) and after (c, d) the interaction

levels of the covalence band (−14.7 and −16.9 eV). The formation of the S1=O bond altered the O 2p states, which interacted with the S 3p state near the Fermi level; the O 2s DOS peaks also overlapped with the S 3s DOS peaks from −23 eV to −10 eV, indicating a hybridization between these orbitals.

4. Conclusions

H_2O_2 could be used as a depressant for pyrite at pH 6.4. The pyrite in the solution enhanced the release of O_2 from H_2O_2, but the O_2 concentration was lower than that of H_2O_2 in the solution. Thus, H_2O_2 is still the major oxidant in the flotation system. The adsorption models of H_2O_2 and O_2 were also compared with DFT calculations. The interaction between H_2O_2 and hydrated pyrite (100) surface produced five stable structures. For the most stable structure, H_2O_2 dissociated into one O atom and an H_2O molecule. This O atom further bonded to an S atom on the surface forming a S=O bond. The reaction of the O_2 molecule with the pyrite (100) surface generated five stable structures. In terms of the most stable structure, the O_2 molecule dissociated into two O atoms, which bonded with S atoms on the hydrated pyrite (100) surface.

Acknowledgments

Financial support from the Analysis and Testing Foundation of Kunming University of Science and Technology (PR China), National Natural Science Foundation of China (22068020), and the Yong Top-notch Talent Project of Yunnan Ten Thousand Talent Plan (Yunnan Province, PR China) is gratefully acknowledged.

References

BAI, X., LIU, J., WEN, S., LIN, Y., 2021. *Effect and mechanism of organic depressant on the hydrophobicity of chalcopyrite and pyrite under weakly alkaline environment*. J. Mater. Res. Technol. 15, 4109-4116.

BAI, X., LIU, J., WEN, S., LIN, Y., 2022. *Selective separation of chalcopyrite and pyrite using a novel organic depressant at low alkalinity.* Miner. Eng. 185, 107677.

CHEN, J., CHEN, Y., LONG, X., LI, Y., 2017. *DFT study of coadsorption of water and oxygen on galena (PbS) surface: An insight into the oxidation mechanism of galena*. Appl. Surf. Sci.., 420, 714-719.

CHEN, J., LAN, L., CHEN, Y., 2013. *Computational simulation of adsorption and thermodynamic study of xanthate, dithiophosphate and dithiocarbamate on galena and pyrite surfaces*. Miner. Eng. **s** 46–47(3), 136–143.

CHEN, J., LI, Y., ZHAO, C., 2014a. *First principles study of the occurrence of gold in pyrite.* Comput. Mater. Sci. 88, 1-6.

CHEN, J., LONG, X., CHEN, Y., 2014. *Comparison of Multilayer Water Adsorption on the Hydrophobic Galena (PbS) and Hydrophilic Pyrite (FeS_2) Surfaces: A DFT Study*. J. Phys. Chem. C. 118, 11657-11665.

CHEN, Y., FENG, B., ZHONG, C., WANG, Z., 2022. *Effect and mechanism of the xanthate/H_2O_2 addition order on flotation separation of chalcopyrite and sphalerite.* Miner. Eng. 188, 107851.

DERYCKE, V., KONGOLO, M., BENZAAZOUA, M., MALLET, M., BARRES, O., DE DONATO, P., BUSSIERE, B., MMERMILLOD-BLONDIN, R., 2013. *Surface chemical characterization of different pyrite size fractions for flotation purposes.* Int. J. Miner. Process. 118, 1-14.

FORSON, P., ZANIN, M., SKINNER, W., ASAMOAH, R., 2021. *Differential flotation of pyrite and arsenopyrite: Effect of hydrogen peroxide and collector type.* Miner. Eng. 163,106808.

FOUCAUD, Y., BADAWI, M., FILIPPOV, L., FILIPOVA, I., LEBEGUE, S., 2019. *A review of atomistic simulation methods for surface physical-chemistry phenomena applied to froth flotation.* Miner. Eng. 143, 106020.

FRANCIS, G.P., PAYNE, M.C, 1990. *Finite basis set corrections to total energy pseudopotential calculations.* J. Phys.: Condens. Matter. 2, 4395-4404.

GISBERT, G., TORNOS, F., LOSANTOS, E., MCLENAGHAN, S., PONS, J.M., VIDEIRA, J.C., BORDBECK, M,. 2022. *Vectors to ore in replacive volcanogenic massive sulphide deposits of the northern Iberian Pyrite Belt: Major and trace element mineral chemistry*. Ore Geol. Rev. 147, 104963.

HAN, R., QIN, K., GROVES, D.I., HUI, K., LI, Z., ZOU, X., LI, G., SU, S., 2022. *Ore-formation at the Halasheng Ag-Pb-Zn deposit, northeast Inner Mongolia as revealed by trace-element and sulfur isotope compositions of ore-related sulfides.* Ore Geol. Rev. 144, 104853.

HONG, G., JUNHYUN, C., HAN, Y., KWANG-SUK, Y., KWANHO, K., BAE, K.S., HYUNJUNG, K., 2017. *Relationship between Surface Characteristics and Floatability in Representative Sulfide Minerals: Role of Surface Oxidation.* Mater. Trans. 58, 1069-1075.

HUANG, T., LEI, S., JI, M., LIU, Y., FAN, Y., 2017. *Density functional theory study of oxygen atom adsorption on different surfaces of pyrite.* J. Wuhan. Univ. Technol. Mater. Sci Ed Sci. Ed., 32(6), 1464-1469.

JAVADI NOOSHABADI, A., LARSSON, A.-C., KOTA, H.R., 2013. *Formation of hydrogen peroxide by pyrite and its influence on flotation*. Miner. Eng. 49, 128-134.

JAVADI NOOSHABADI, A., RAO, K.H., 2016. *Complex sulphide ore flotation: Effect of depressants addition during grinding on H_2O_2 formation and its influence on flotation.* Int. J. Miner. Process, 157, 89-97.

JIN, J., MILLER, J.D., DANG, L.X., WICK, C.D., 2015. *Effect of surface oxidation on interfacial water structure at a pyrite (100) surface as studied by molecular dynamics simulation.* Int. J. Miner. Process. 139, 64-76.

JIN, J., WANG, X., GAO, P., LIU, J., ZHU, Y., HAN, Y., 2021. *Selective adsorption behavior and mechanism of a high-performance depressant in the flotation separation of pyrite from talcum.* J. Mol. Liq. 325, 114707.

KHOSO, S.A., GAO, Z., SUN, W., 2021. *Recovery of high-grade copper concentrate from sulfur-rich porphyry ore using tricarboxystarch micromolecule as pyrite depressant*. Miner. Eng. 168, 106916.

KHOSO, S.A., HU, Y., LÜ, F., GAO, Y., LIU, R., SUN, W., 2019. *Xanthate interaction and flotation separation of H_2O_2-treated chalcopyrite and pyrite.* T Nonferr Metal Soc. 29, 2604-2614.

KHOSO, S.A., HU, Y., LYU, F., LIU, R., SUN, W.,2019b, *Selective separation of chalcopyrite from pyrite with a novel non-hazardous biodegradable depressant.* J. Cleaner Prod. 232, 888-897.

LU, C., WANG, Y., QIAN, P., LIU, Y., FU, G., DING, J., YE, S., CHEN, Y., 2018. *Separation of chalcopyrite and pyrite from a copper tailing by ammonium humate.* Chin. J. Chem. Eng. 26(9), 1814-1821.

LI, Y., CHEN, J., CHEN, Y., GUO, J., 2011. *Density functional theory study of influence of impurity on electronic properties and reactivity of pyrite.* T. Nonferr. Metal. Soc, 21(8), 1887-1895.

LI, Y., CHEN, J., CHEN, Y., ZHAO, C., LEE, M. –H., LIN, T.-H., 2018. *DFT+U study on the electronic structures and optical properties of pyrite and marcasite.* Comput. Mater. Sci., 150, 346-352.

LIU, D., YI, M., YANG, S., LIIU, F., LI, Y., 2022. *Performance and mechanism of the pyrite-kerogen complexes oxidation with H2O2 at low temperature during shale stimulation: An experimental and modeling study.* Appl. Geochem. 143, 105382.

LIU, D., ZHANG, G., CHEN, Y., 2021. *Studies on the selective flotation of pyrite from fine serpentine by using citric acid as depressant.* Miner. Eng. 165, 106742.

MU, Y., PENG, Y., LAUTEN, R.A., 2016. *The depression of pyrite in selective flotation by different reagent systems – A Literature review.* Miner. Eng. 96-97, 143-156.

Muravyov, M., 2019. *Bioprocessing of mine waste: effects of process conditions*. Chem. Pap. 73, 3075-3083.

PERDEW, J.P., BURKE, K., ERNZERHOF, M., 1996. *Generalized Gradient Approximation Made Simple.* Phys. Rev. Lett 7:3865-3868.

PERDEW, J.P., ZUNGER, A., 1981. *Self-interaction correction to density-functional approximations for many-electron systems.* Phys. Rev. B. 23, 5048.

PERRON, H., VANDENBORRE, J., DOMAIN, C., DROT, R., ROQUES, J., SIMONI, E., EHRHARDT, J.J., CATALETTE, H., 2007. *Combined investigation of water sorption on TiO_2 rutile (1 1 0) single crystal face: XPS vs. periodic DFT.* Surf. Sci. 601, 518-527.

ROZGONYI, T., STIRLING, A., 2015. *DFT Study of Oxidation States on Pyrite Surface Sites*. J. Phys. Chem. C. 119, 7704-7710.

SEGALL, M., LINDAN, P.J., PROBERT, M.A., PICKARD, C., HASNIP, P., CLARK, S., PAYNE, M., 2002. *First-principles simulation: ideas, illustrations and the CASTEP code.* J. Phys.: Condens. Matter. 14, 2717.

SUYANTARA, G.P.W., HIRAJIMA, T., MIKI, H., SAKAKI, K., YAMANE, M., TAKIDA, E., KUROIWA, S., IMAIZUMI, Y., 2018. *Selective flotation of chalcopyrite and molybdenite using H2O2 oxidation method with the addition of ferrous sulfate.* Miner. Eng. 122, 312-326.

TARCHOUNA, Y., BAHRI, M., JAIDANE, N., LAKHDAR, Z.B., 2006. *Kinetic study of the hydrogen abstraction reaction $H_2O_2+H\rightarrow H_2+HO_2$ by ab initio and density functional theory calculations.* J. Mol. Struct.: THEOCHEM. 758, 53-60.

YANG, X., LI Y., FANR., DUAN, W., HUANG, L., XIAO, Q., 2022. *Separation mechanism of chalcopyrite and pyrite due to H2O2 treatment in low-alkaline seawater flotation system.* Miner. Eng. 176, 107356.

ZHANG, H., ZHANG, F., SUN, W., CHEN, D., CHEN, J., WWANG R., HAN, M., ZHANG, C., 2023. *The effects of hydroxyl on selective separation of chalcopyrite from pyrite: A mechanism study.* Appl. Surf. Sci. 608, 154963.

ZHANG, P., HUANG, W., JI, Z., ZHOU, C., YUAN, S., 2018. *Mechanisms of hydroxyl radicals production from pyrite oxidation by hydrogen peroxide: Surface versus aqueous reactions.* Geochim. Cosmochim. Acta. 238, 394-410.